JACS
JOURNAL OF THE AMERICAN CHEMICAL SOCIETY
Communication
pubs.acs.org/JACS
Terms of Use

The Cyanide Ligands of [FeFe] Hydrogenase: Pulse EPR Studies of ^{13}C and ^{15}N-Labeled H-Cluster

William K. Myers,[†,§] Troy A. Stich,[†,§] Daniel L. M. Suess,[†] Jon M. Kuchenreuther,[†] James R. Swartz,[‡] and R. David Britt*[,†]

[†]Department of Chemistry, University of California, Davis, Davis, California 95616 United States

[‡]Department of Chemical Engineering and Department of Bioengineering, Stanford University, Stanford, California 94305 United States

Supporting Information

ABSTRACT: The two cyanide ligands in the assembled cluster of [FeFe] hydrogenase originate from exogenous L-tyrosine. Using selectively labeled tyrosine substrates, the cyanides were isotopically labeled via a recently developed *in vitro* maturation procedure allowing advanced electron paramagnetic resonance techniques to probe the electronic structure of the catalytic core of the enzyme. The ratio of the isotropic ^{13}C hyperfine interactions for the two CN^- ligands—a reporter of spin density on their respective coordinating iron ions—collapses from ≈5.8 for the H_{ox} form of hydrogenase to <2 for the CO-inhibited form. Additionally, when the maturation was carried out using [^{15}N]-tyrosine, no features previously ascribed to the nitrogen of the bridging dithiolate ligand were observed suggesting that this bridge is not sourced from tyrosine.

Hydrogenases catalyze the redox interconversion of protons and H_2 and thus have received much focus as key elements in biological solar fuel production.[1] The [FeFe] form of hydrogenase (HydA) is particularly active,[1] and its catalytic H-cluster consists of a [4Fe-4S] cluster ($[4Fe\text{-}4S]_H$) linked through a cysteine sulfur to a unique dinuclear iron cluster ($[FeFe]_H$, Scheme 1).[2] This subcluster possesses five inorganic ligands—two CN^- and three CO—as well as a bridge recently assigned as dithiomethylamine (DTMA).[3,4]

Active HydA can be expressed in *Escherichia coli* only by also adding genes for three Fe-S containing maturase enzymes—HydE, HydF, and HydG—that are required for production of the $[FeFe]_H$ subcluster.[5] Alternatively, synthetic dinuclear Fe clusters can be transferred to HydA apoprotein (containing only the $[4Fe\text{-}4S]_H$ subcluster) to produce active enzyme.[4] We are utilizing a different technology: the HydE, HydF, and HydG maturases are added to a solution of apo-HydA for *in vitro* maturation and concurrent activation.[6] This cell-free biosynthetic method allows for facile and precise isotope incorporation into the $[FeFe]_H$ subcluster.[7]

The Fe-bound CO and CN^- ligands of the $[FeFe]_H$ subcluster are sourced from L-tyrosine (Tyr) and produced by HydG.[8−10] In the present study, we use the cell-free biosynthetic method along with α-^{13}C-Tyr ([2-^{13}C]-Tyr) and [^{15}N]-Tyr to specifically label the two CN^- ligands with the magnetic nuclei ^{13}C and ^{15}N (I = 1/2).[11,12] The hyperfine interaction (HFI) of these magnetic nuclei with the unpaired electrons distributed over the H-cluster serve as site-specific reporters of its electronic structure, important metrics for evaluating computational models of the H-cluster.

When poised in the active oxidation state known as H_{ox}, the $[4Fe\text{-}4S]_H$ subcluster is diamagnetic with a formal charge of 2+,[13] though the $[4Fe\text{-}4S]_H$ carries some unpaired density due to the exchange interaction with the $[FeFe]_H$ fragment. $[FeFe]_H$ itself is in a formally mixed-valence Fe(I,II) S = 1/2 state that is characterized by a rhombic electron paramagnetic resonance (EPR) spectrum (Figure 1A, top). While the overall oxidation state of the H_{ox} form of the H-cluster is widely accepted, the distribution of the valences about the cluster is still debated. One formulation based on results from electronic structure calculations assigns a 1+ oxidation state to the Fe that is distal to the $[4Fe\text{-}4S]_H$ subcluster (Fe_d), leaving the proximal Fe ion (Fe_p) in the ferrous oxidation state.[14] However, ^{57}Fe electron nuclear double resonance (ENDOR) spectroscopic studies of HydA from *Desulfovibrio desulfuricans* (*DdS*) found that the spin density was shared more-or-less equally over both iron ions of $[FeFe]_H$.[15] Many computational models of the H-cluster have been judged based on the quality of the predicted magnetic parameters. Initially, only the ^{57}Fe HFI were employed as a discriminating constraint.[14,16] More recently, however, ligand HFI, from either the nearby, naturally abundant ^{14}N nuclei or from ^{13}C nuclei introduced by treatment of HydA with isotopically labeled ^{13}CO gas, have been used to evaluate computer-generated structural models of the H-cluster.[3,16,17] Unfortunately, in the case of the ^{14}N hyperfine parameters, the assignment of the observed signals to

Scheme 1

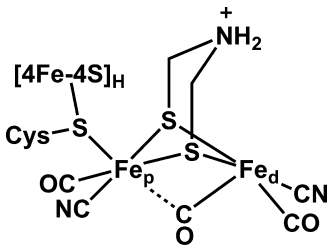

Received: July 11, 2014
Published: August 15, 2014

dx.doi.org/10.1021/ja507046w | J. Am. Chem. Soc. 2014, 136, 12237−12240

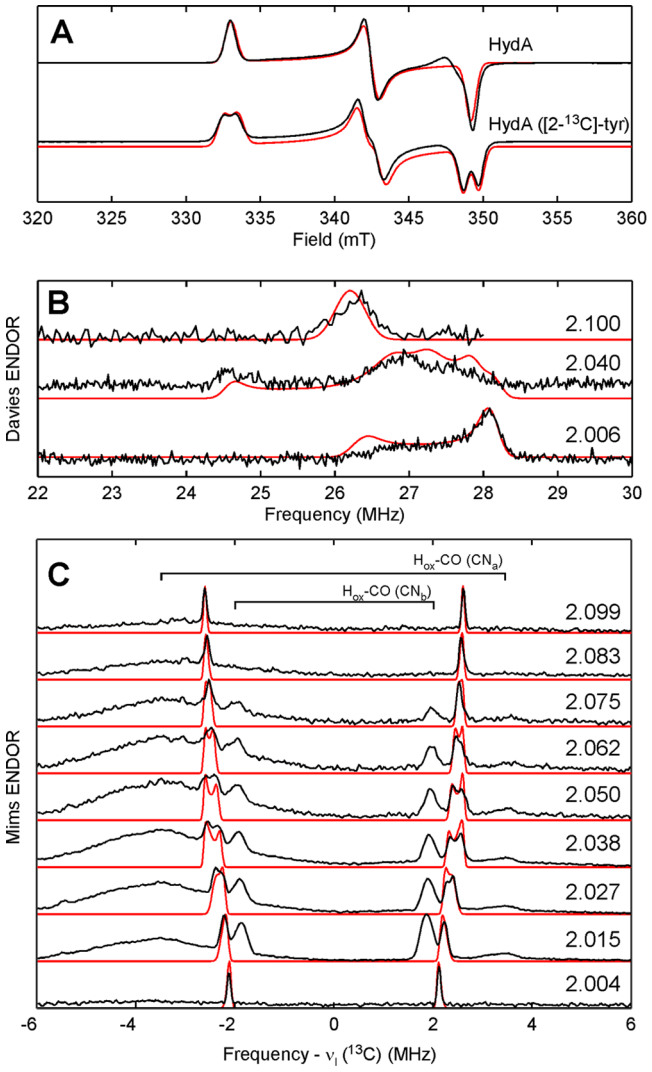

Figure 1. X-band (9.4 GHz) CW EPR spectra (A) of the H_{ox} form of HydA matured using natural-abundance Tyr (top) or [2-^{13}C]-Tyr (bottom). Davies ENDOR spectra (B) of HydA ([2-^{13}C]-Tyr) collected at 1158, 1192, and 1212 mT (top to bottom). Corresponding *g*-values given in figure. Q-band (33.79 GHz) Mims ENDOR spectra (C) of HydA ([2-^{13}C]-Tyr) collected at 1150, 1157, 1164, 1171, 1178, 1184, 1191, 1198, and 1205 mT (top to bottom). Corresponding *g*-values given in figure. Traces of experimental data are shown in black; simulations for the H_{ox} form are presented in red.

specific nitrogen atoms is ambiguous owing to the high natural-abundance of ^{14}N; and the ^{13}CO-treatment aids only in characterizing the H_{ox}-CO form. We therefore reasoned that studies of the electronic structure of H_{ox} would be aided by selective incorporation of magnetic nuclei into the diatomic ligands of the $[FeFe]_H$ cluster.

The X-band continuous-wave (CW) EPR spectrum of *in vitro* matured HydA from *Clostridium pasteurianum* (CpI) poised in the H_{ox} state is consistent with that published previously with *g* = 2.100, 2.040, 1.996 (Figure 1A). Using [2-^{13}C]-Tyr in the maturation of HydA leads to a splitting of ≈1 mT centered at each *g*-value of this H_{ox} signal (cf. top and bottom traces in Figure 1A).[18] Q-band Davies ENDOR spectra acquired at field positions corresponding to each *g*-value (Figure 1B) confirm this strong ^{13}C HFI by showing features at ≈27 MHz that have no counterpart in analogous spectra of HydA matured using natural-abundance tyrosine.[19] The variation in shape and breadth of these features as a function of resonant field position results from orientation selection, i.e., at certain field positions, a discrete subset of molecular orientations of HydA are probed. Proper simulation of this behavior allows for the orientation of the corresponding ^{13}C hyperfine tensor to be determined relative to the molecular *g*-tensor. These parameters are summarized in Table 1. The degree of ^{13}C HFI anisotropy is consistent with that of other Fe-bound cyanides (cf. Table 1).

Orientation-selected Mims ENDOR spectra (Figure 1C) reveal three distinct classes of more weakly coupled ^{13}C nuclei (A_{iso} = 3.80, 4.87, and ≈7.0 MHz). These features are centered about the ^{13}C Larmor frequency and split by the magnitude of the HFI. Analogous data sets collected for CO-treated samples (Figures S3 and S4) possess similar features at ±1.8 and ±3.6 MHz, confirming that they arise from the two cyanide ligands in the H_{ox}-CO form of hydrogenase (labeled as CN_a and CN_b since we cannot distinguish between the Fe_p-bound and Fe_d-bound cyanides at this time). Note the absence of contributions from H_{ox}-CO to the ENDOR spectra acquired at the extreme field positions (*g* = 2.099 and 2.004) of H_{ox} (Figure 1C). This results from the relative narrowness of the H_{ox}-CO signal. This narrowness is also why we see strong contributions from H_{ox}-CO even though the contamination is relatively small. The remaining features centered at ±2.2 MHz in Figure 1C are thus ascribed to the other CN^- ligand in H_{ox}.

Based on the crystallographic results,[2] Fe_d possesses a square pyramidal local geometry whose *z*-axis points along the bond between the Fe_d ion and the bridging CO. For the six-coordinate Fe_p, the identity of the local *z*-axis is less obvious, but computational results suggest that it is aligned along the Fe_p-CO_{bridge} bond.[14] As the two terminal CN^- ligands appear to be bound in the same position relative to the local *z*-axis of their respective Fe ions, the ratio of the isotropic ^{13}C HFI should serve as a reporter of the relative spin density on each iron. Again, based on earlier computational results, we assign the larger ^{13}C HFI as arising from the distal Fe-bound cyanide of H_{ox}. For the proximal Fe-bound cyanide, we measure A_{iso} = 4.87 MHz. This ratio of ≈5.8 correlates approximately with the Fe_d:Fe_p ratio of computed Mulliken spin populations.[14,16] For H_{ox}–CO, the $A_{iso}(^{13}CN_a)$:$A_{iso}(^{13}CN_b)$ ratio drops to <2 (see magnetic parameters listed in Table 1) indicating a much more even distribution of spin density over the two Fe ions than what was observed for H_{ox} that is again consistent with computational results.[14,16] Interestingly, the ^{13}C HFI tensors for the two CN^- ligands in the H_{ox}–CO form lack significant anisotropy compared to other Fe-bound cyanides (cf. Table 1)

X- and Q-band HYSCORE spectra for natural-abundance H_{ox} (Figure 2, top) are essentially identical to those obtained earlier by Silakov et al.[3] When the *in vitro* maturation of HydA is performed with ^{15}N-labeled tyrosine ([^{15}N]-Tyr), the nitrogens of the cyanide ligands become selectively isotopically labeled.[9] The corresponding HYSCORE data are strikingly different from those of natural-abundance H_{ox} (cf. top and bottom plots in Figure 2) signaling that the majority of features arise from tyrosine-derived nitrogens. The correlation ridges in the Q-band spectrum of H_{ox} ([^{15}N]-Tyr) are well-simulated with the hyperfine parameters $A(^{15}N)$ = [0.8, 6.3, −1.2] MHz (Figure S5). Given the rather large magnitude of $A_{iso}(^{15}N)$, this nitrogen is likely that in the Fe_d-bound cyanide. We observe no ^{15}N-derived features that we could assign to cyanides in the H_{ox}–CO form.

dx.doi.org/10.1021/ja507046w | J. Am. Chem. Soc. 2014, 136, 12237−12240

Table 1. ^{13}C HFI and ^{15}N HFI for CO and CN Bound to Fe-Centers

species	A^{13}C (MHz)	[α, β, γ] (deg)[a]	assignment	reference
CpI H_{ox} ([2-^{13}C]-Tyr)	[30.9, 23.3, 30.2]	[60, 120, 170]	CN_d	this work
	[5.22, 5.24, 4.16]	[30, 90, 0]	CN_p	this work
CpI H_{ox}-CO ([2-^{13}C]-Tyr)	[7.0, 7.0, 7.2]	[0, 0, 0]	CN_a	this work
	[3.75, 3.75, 3.90]	[0, 0, 0]	CN_b	this work
DdS H_{ox}-^{13}CO	[15.6, 16.6, 19.2]		CO_{ext}	17
	[8.5, 9.8, 3.9]		CO_{bridge}	17
	[3.2, 3.7, 4.4]		CO_d	17
Mb-^{13}CN	[−23.0, −27.6, −28.7]		Fe(III)-CN	21
Pf Fd-^{13}CN	[−4.5, −4.5, +0.1]		[4Fe-4S]$^+$-CN	22
species	A^{15}N (MHz)	[α, β, γ] (deg)	assignment	reference
CpI H_{ox} ([^{15}N]-Tyr)	[0.8, 6.3, −1.2]	[45, −20, 0]	CN_d	this work
DdS H_{ox}	[2.1, 5.3, −0.6][b]	[41, 24, 0]	CN_d	3
	[1.4, 2.7, 2.0][b]	[40, 25, 0]	DTMA	3
	[−3.4, 2.0, −1.0][b]	[0, 4, 20]	Lys	3
DdS H_{ox}-CO	[0.56, −0.28, 0.79][b]	[0, −10, 0]		17
Mb-C^{15}N	[n.d., n.d., 5.25]		Fe(III)-CN	23
Pf Fd-C^{15}N	[+1.8, +1.0, −2.4]		[4Fe-4S]$^+$-CN	22

[a]Euler angles are relative to *g*-frame defined by $g1 < g2 < g3$. For H_{ox}, this corresponds to $g_z < g_y < g_x$ as we assign the local *z*-axis of Fe_d to the Fe-CO_{bridge} bonding vector. [b]Determined by scaling the experimentally determined ^{14}N HFI by the ratio of the ^{15}N/^{14}N Larmor frequencies (1.4028). [c]Abbreviations: Mb = myoglobin; *Pf* Fd = [4Fe-4S] ferredoxin from *Pyrococcus furiosus*; n.d. = not determined.

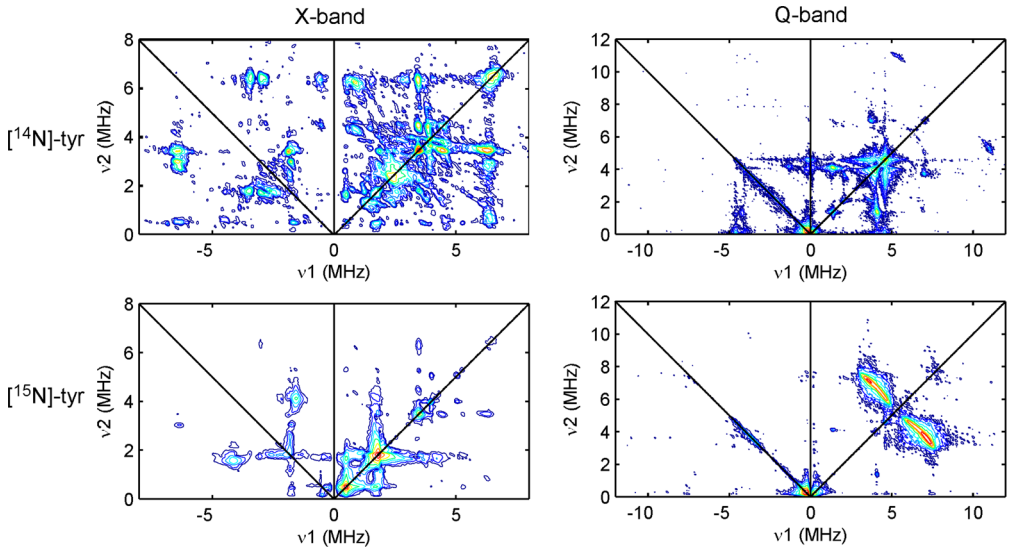

Figure 2. X-band (left) and Q-band (right) HYSCORE spectra of the H_{ox} form of HydA matured using natural-abundance ([^{14}N]-Tyr, top) or with [^{15}N]-Tyr (bottom).

The biosynthetic origin of the putative DTMA bridge is presently unknown. One proposal suggests that HydG can assemble this bridging ligand from two molecules of tyrosine.[20] Analysis of ^{14}N HYSCORE spectra of *DdS* HydA poised in the H_{ox} state led to the assignment of a set of correlation ridges to the DTMA amino nitrogen ($A(^{14}N)$ = [1.0, 1.9, 1.4] MHz).[3] By scaling this reported ^{14}N HFI by the ratio of the ^{15}N/^{14}N Larmor frequencies, we can simulate the X-band HYSCORE spectrum as if the DTMA had been ^{15}N-labeled (see Figures S6 and S7). The predicted correlation ridges corresponding to the ^{15}N-DTMA nitrogen are not found in the experimental HYSCORE spectrum of H_{ox} ([^{15}N]-Tyr) suggesting either that tyrosine is not the source of the DTMA nitrogen or that the previously reported ^{14}N HFI parameters for *DdS* HydA are not appropriate for CpI H_{ox}.

Using isotopically labeled tyrosine substrates in conjunction with the *in vitro* biosynthetic route to generate the H-cluster gives us the flexibility to site-specifically label the cyanide ligands with ^{13}C and ^{15}N. The signals we observe from ^{15}N are unambiguously attributed to the nitrogen of an Fe-bound cyanide. Further, comparison of the two cyanide ^{13}C couplings is consistent with just one of the Fe ions (Fe_d) of $[FeFe]_H$ carrying the majority of unpaired electron spin in the H_{ox} state. As such, the relatively large rhombicity of the H_{ox} EPR signal can be understood as arising from the asymmetry in the equatorial ligand set for the low-spin $3d^7$ Fe_d spin center. Thus, the difference in *g*-shifts for g_y and g_x (0.0367 vs 0.0947) is attributed to the difference in the energies of the Fe_d-$3d_{xz}$ → Fe_d-$3d_{z^2}$ and the Fe_d-$3d_{yz}$ → Fe_d-$3d_{z^2}$ transitions, respectively.[24] If we orient the *g*-tensor for H_{ox} as follows: g_z is oriented along of *z*-axis of Fe_d, and g_x and g_y are made to bisect the Fe_d-S and Fe_d-S bonding vectors and the Fe_d-CO_d and Fe_d-CN_d bonding vectors, respectively; then the unique axis of the ^{13}C hyperfine tensor for CN_d is found to point approximately along the Fe_d-

dx.doi.org/10.1021/ja507046w | J. Am. Chem. Soc. 2014, 136, 12237−12240

CN_d bond, as expected (Figure S8).[25] This finding supports our electronic structure description of H_{ox}; namely, that the unpaired electron largely resides in a molecular orbital of $3d_{z^2}$ character centered on the Fe_d ion.

Based on the similar magnitudes of the ^{13}CN HFI, the electron spin becomes distributed more evenly over both iron ions after inhibition with free CO. This more delocalized spin topology leads to a collapse of the *g*-matrix rhombicity. Analogously, the rather narrow EPR signal for the formally mixed-valence Cu(I,II) Cu_A cluster in nitrous oxide reductase is understood as a weighted sum of the hypothetical mononuclear *g*-matrices of each Cu site.[26] In the case of H_{ox}-CO, we do not know the values for the intrinsic *g*-matrix for the two Fe ions. However, we can use the H_{ox} *g*-values as a first estimate. Upon forming H_{ox}-CO, delocalization of the unpaired electron spin cancels out some of the anisotropy from each site-specific *g*-matrix, leading to the axial (g = 2.072, 2.006, 2.006), molecular *g*-matrix. The nearly isotropic HFI tensors for the two CN^- ligands in H_{ox}-CO result from this same mechanism of anisotropy cancellation. These findings are in agreement with earlier computational models[14,16] that indicate a dramatic delocalization of unpaired spin density in going from the H_{ox} form to H_{ox}-CO

■ ASSOCIATED CONTENT

Supporting Information

Details of experimental procedures and data analysis methods. Supplemental EPR spectra and corresponding simulations. This material is available free of charge via the Internet at http://pubs.acs.org.

■ AUTHOR INFORMATION

Corresponding Author

rdbritt@ucdavis.edu

Author Contributions

[§]These authors contributed equally.

Notes

The authors declare no competing financial interest.

■ ACKNOWLEDGMENTS

This work was funded by National Institutes of Health (GM104543 to R.D.B.) and the Division of Material Sciences and Engineering (J.R.S. award no. DE-FG02-09ER46632) of the Office of Basic Energy Sciences of the U.S. Department of Energy. D.L.M.S. acknowledges support from the National Institutes of Health (F32GM111025 from the NIGMS).

■ REFERENCES

(1) Vincent, K. A.; Parkin, A.; Armstrong, F. A. *Chem. Rev.* **2007**, *107*, 4366.

(2) Peters, J. W.; Lanzilotta, W. N.; Lemon, B. J.; Seefeldt, L. C. *Science* **1998**, *282*, 1853.

(3) Silakov, A.; Wenk, B.; Reijerse, E.; Lubitz, W. *Phys. Chem. Chem. Phys.* **2009**, *11*, 6592.

(4) Berggren, G.; Adamska, A.; Lambertz, C.; Simmons, T. R.; Esselborn, J.; Atta, M.; Gambarelli, S.; Mouesca, J. M.; Reijerse, E.; Lubitz, W.; Happe, T.; Artero, V.; Fontecave, M. *Nature* **2013**, *499*, 66.

(5) Shepard, E. M.; Mus, F.; Betz, J. N.; Byer, A. S.; Duffus, B. R.; Peters, J. W.; Broderick, J. B. *Biochemistry* **2014**, *53*, 4090.

(6) Kuchenreuther, J. M.; Shiigi, S. A.; Swartz, J. R. *Methods Mol. Biol. (N. Y., NY, U. S.)* **2014**, *1122*, 49.

(7) Kuchenreuther, J. M.; Myers, W. K.; Suess, D. L. M.; Stich, T. A.; Pelmenschikov, V.; Shiigi, S. A.; Cramer, S. P.; Swartz, J. R.; Britt, R. D.; George, S. J. *Science* **2014**, *343*, 424.

(8) Swanson, K. D.; Duffus, B. R.; Beard, T. E.; Peters, J. W.; Broderick, J. B. *Eur. J. Inorg. Chem.* **2011**, 935.

(9) Kuchenreuther, J. M.; George, S. J.; Grady-Smith, C. S.; Cramer, S. P.; Swartz, J. R. *PLoS One* **2011**, *6*, e20346.

(10) Kuchenreuther, J. M.; Myers, W. K.; Stich, T. A.; George, S. J.; NejatyJahromy, Y.; Swartz, J. R.; Britt, R. D. *Science* **2013**, *342*, 472.

(11) Driesener, R. C.; Challand, M. R.; McGlynn, S. E.; Shepard, E. M.; Boyd, E. S.; Broderick, J. B.; Peters, J. W.; Roach, P. L. *Angew. Chem.* **2010**, *49*, 1687.

(12) Shepard, E. M.; Duffus, B. R.; George, S. J.; McGlynn, S. E.; Challand, M. R.; Swanson, K. D.; Roach, P. L.; Cramer, S. P.; Peters, J. W.; Broderick, J. B. *J. Am. Chem. Soc.* **2010**, *132*, 9247.

(13) Popescu, C. V.; Munck, E. *J. Am. Chem. Soc.* **1999**, *121*, 7877.

(14) Fiedler, A. T.; Brunold, T. C. *Inorg. Chem.* **2005**, *44*, 9322.

(15) Silakov, A.; Reijerse, E. J.; Albracht, S. P. J.; Hatchikian, E. C.; Lubitz, W. *J. Am. Chem. Soc.* **2007**, *129*, 11447.

(16) Greco, C.; Silakov, A.; Bruschi, M.; Ryde, U.; De Gioia, L.; Lubitz, W. *Eur. J. Inorg. Chem.* **2011**, 1043.

(17) Silakov, A.; Wenk, B.; Reijerse, E.; Albracht, S. P. J.; Lubitz, W. *J. Biol. Inorg. Chem.* **2009**, *14*, 301.

(18) A modest (20% of overall spectral intensity) of the axial signal (g = 2.072, 2.006, 2.006) arising from H_{ox}-CO was removed by subtraction. H_{ox}-CO contamination is common and can be seen by other methods such as infrared absorption spectroscopy.[9]

(19) This ENDOR transition at 27 MHz is approximately equal to twice the ^{13}C Larmor frequency at this field; therefore the ENDOR transtion in other spin manifold is expected at <1 MHz though it is not evident in our ENDOR data. However, both ^{13}C spin-flip transitions are observed in the Q-band HYSCORE spectrum (Figure S2).

(20) Pilet, E.; Nicolet, Y.; Mathevon, C.; Douki, T.; Fontecilla-Camps, J. C.; Fontecave, M. *FEBS Lett.* **2009**, *583*, 506.

(21) Van Doorslaer, S.; Trandafir, F.; Harmer, J. R.; Moens, L.; Dewilde, S. *Biophys. Chem.* **2014**, *190*−*191*, 8.

(22) Telser, J.; Smith, E. T.; Adams, M. W. W.; Conover, R. C.; Johnson, M. K.; Hoffman, B. M. *J. Am. Chem. Soc.* **1995**, *117*, 5133.

(23) Mulks, C. F.; Scholes, C. P.; Dickinson, L. C.; Lapidot, A. *J. Am. Chem. Soc.* **1979**, *101*, 1645.

(24) Weil, J. A.; Bolton, J. R. *Electron paramagnetic resonance: elementary theory and practical applications*; John Wiley & Sons: Hoboken, NJ, 2007.

(25) Telser, J.; Smith, E. T.; Adams, M. W. W.; Conover, R. C.; Johnson, M. K.; Hoffman, B. M. *J. Am. Chem. Soc.* **1995**, *117*, 5133.

(26) Neese, F.; Zumft, W. G.; Antholine, W. E.; Kroneck, P. M. H. *J. Am. Chem. Soc.* **1996**, *118*, 8692.